2017

Mo2C/CNT: An Efficient Catalyst for Rechargeable Li–CO2 Batteries

Yuyang Hou
University of Wollongong, yh879@uowmail.edu.au

Jiazhao Wang
University of Wollongong, jiazhao@uow.edu.au

Lili Liu
University of Wollongong, ll422@uowmail.edu.au

Yuqing Liu
University of Wollongong, yl037@uowmail.edu.au

Shulei Chou
University of Wollongong, shulei@uow.edu.au

See next page for additional authors

Publication Details

Hou, Y., Wang, J., Liu, L., Liu, Y., Chou, S., Shi, D., Liu, H., Wu, Y., Zhang, W. & Chen, J. (2017). Mo2C/CNT: An Efficient Catalyst for Rechargeable. Advanced Functional Materials, 27 1700564-1-1700564-8.

Mo2C/CNT: An Efficient Catalyst for Rechargeable Li–CO2 Batteries

Abstract
The rechargeable Li-CO2 battery is a novel and promising energy storage system with the capability of CO2 capture due to the reversible reaction between lithium ions and carbon dioxide. Carbon materials as the cathode, however, limit both the cycling performance and the energy efficiency of the rechargeable Li-CO2 battery, due to the insulating Li2CO3 formed in the discharge process, which is difficult to decompose in the charge process. Here, a Mo2C/carbon nanotube composite material is developed as the cathode for the rechargeable Li-CO2 battery and can achieve high energy efficiency (77%) and improved cycling performance (40 cycles). A related mechanism is proposed that Mo2C can stabilize the intermediate reduction product of CO2 on discharge, thus preventing the formation of insulating Li2CO3. In contrast to insulating Li2CO3, this amorphous Li2C2O4-Mo2C discharge product can be decomposed below 3.5 V on charge. The introduction of Mo2C provides an effective solution to the problem of low round-trip efficiency in the Li-CO2 battery.

Keywords
catalyst, rechargeable, mo2c/cnt:, efficient

Disciplines
Engineering | Physical Sciences and Mathematics

Publication Details
Hou, Y., Wang, J., Liu, L., Liu, Y., Chou, S., Shi, D., Liu, H., Wu, Y., Zhang, W. & Chen, J. (2017). Mo2C/CNT: An Efficient Catalyst for Rechargeable. Advanced Functional Materials, 27 1700564-1-1700564-8.

Authors
Yuyang Hou, Jiazhao Wang, Lili Liu, Yuqing Liu, Shulei Chou, Dongqi Shi, Hua-Kun Liu, Yu-Ping Wu, Weimin Zhang, and Jun Chen

WILEY-VCH

DOI: 10.1002/((please add manuscript number))

Mo_2C/CNT - An Efficient Catalyst for Rechargeable Li-CO_2 Batteries

Yuyang Hou[1], Jiazhao Wang[2,], Lili Liu[2], Yuqing Liu[1], Shulei Chou[2], Dongqi Shi[2], Huakun Liu[2], Yuping Wu[3], Weimin Zhang[4], Jun Chen[1,*]*

Y. Hou, Y. Liu, Prof. J. Chen
Intelligent Polymer Research Institute
ARC Centre of Excellence for Electromaterials Science
University of Wollongong
Wollongong, NSW 2522, Australia
E-mail: junc@uow.edu.au

Dr. L. Liu, Dr. S. Chou, Dr. D. Shi, Prof. H. Liu, Prof. J. Wang
Institute for Superconducting and Electronic Materials
University of Wollongong
Wollongong, NSW 2522, Australia
E-mail: Jiazhao@uow.edu.au

Prof. Y. Wu
School of Energy Science and Engineering & Institute of Electrochemical Energy Storage
Nanjing Tech University
Nanjing 211816, Jiangsu Province, China

Associate Prof. W. Zhang
Shanghai Electrochemical Energy Devices Research Center
School of Chemistry and Chemical Engineering, Shanghai Jiao Tong University
Shanghai 200240, China

Keywords: molybdenum carbide, cathode materials, interface reaction, electrocatalysis, Li-CO_2 batteries.

Abstract

The rechargeable Li-CO_2 battery is a novel and promising energy storage system with the capability of CO_2 capture due to the reversible reaction between lithium ions and carbon dioxide. Carbon materials as cathode, however, limit both the cycling performance and the energy efficiency of the rechargeable Li-CO_2 battery, due to the insulating Li_2CO_3 formed in the discharge process, which is difficult to decompose in the charge process. Herein, Mo_2C/carbon nanotube (CNT) composite material is developed as the cathode for the rechargeable Li-CO_2 battery, which can achieve high energy efficiency (77%) and improved cycling performance (40 cycles). The related mechanism is proposed, that Mo_2C can stabilize the intermediate reduction product of CO_2 on discharge, thus preventing the formation of insulating Li_2CO_3. In contrast to insulating Li_2CO_3, this amorphous $Li_2C_2O_4$-Mo_2C discharge product could be decomposed below 3.5 V on charge. The introduction of Mo_2C provides an effective solution to the problem of low round-trip efficiency in the Li-CO_2 battery.

1. Introduction

Due to the increasingly serious greenhouse effect on the global climate, the increasing CO_2 content in the atmosphere has received significant attention in recent years. As a result, a number of technologies, including CO_2 capture, conversion, and electrochemical reduction, have been developed to control the concentration of CO_2 in the atmosphere.[1–4] To find a method to utilize CO_2, the strategy of enhancing the discharge capacity of the Li-air battery by combining CO_2 with oxygen was proposed.[5] The formation of Li_2CO_3 during the discharge process can be seen as a novel method to capture and utilize CO_2, but the difficult electrochemical decomposition of Li_2CO_3 has limited its use as a secondary battery. In the light of this, a primary Li-CO_2 battery was reported as a novel method for CO_2 capture and utilization, which showed a tremendous enhancement at 100 °C compared with its performance at low temperature.[6] Recently, Lim *et al*. found that the electrochemical activation of CO_2 within the high dielectric medium of dimethyl sulfoxide (DMSO) led to Li_2CO_3 as a side product of Li-O_2 batteries, which was formed and decomposed reversibly.[7] On the basis of this reversible reaction of Li_2CO_3, a rechargeable Li-CO_2 battery was first proposed as a novel battery and CO_2 conversion device.[8] The utilization of this greenhouse gas in electrochemical energy storage systems provides a promising environmental friendly strategy for reducing fossil fuel energy consumption and slowing global warming.[9-11] Moreover, this kind of metal-CO_2 battery has the potential to become the energy source for scientific exploration and future immigration to Mars in the long run, since the atmosphere of Mars is composed mostly of carbon dioxide.[11] In addition, with the presence of CO_2 in ambient air, it is still a challenge to develop Li-air batteries, since Li_2CO_3 is formed upon discharge as the side product. Only through a better understanding of the mechanism of the Li-CO_2 battery can we hope realize expansion of the application of the Li-O_2 battery to the Li-air battery.[12]

Carbon materials have been extensively utilized as the cathode materials in the rechargeable Li-CO_2 batteries investigated so far, mainly because of their adequate electrical conductivity and large surface area.[8,13,14] According to previous experimental results, rechargeable Li-CO_2 batteries were realized based on the reversible reaction: $4Li + 3CO_2 \leftrightarrow 2Li_2CO_3 + C$.[6,8] This electrochemical reaction shows that lithium ions combine with electrons and CO_2 to form Li_2CO_3 and carbon during discharge in the forward reaction, and Li_2CO_3 combines with carbon to release lithium ions, electrons and CO_2 during charge in the backward reaction. It was also calculated that the theoretical potential is about 2.8 V, based on the formula $E = -\Delta_r G/nF$, in which $\Delta_r G$ represents the change in Gibbs free energy, n is the electron transfer number, and F is the Faraday constant.[6] Unfortunately, Li_2CO_3 is a wide band-gap insulator and insoluble in this aprotic system. As a result, Li_2CO_3 is deposited on the cathode and accumulates upon discharge, leading to an increase in the impedance up to a "sudden death", similar to the case of Li_2O_2 deposits during discharge in the aprotic Li-O_2 battery, which causes a high overpotential for Li_2O_2 decomposition during charge process. Therefore, it is essential to develop new cathode materials to reduce this high charge potential plateau and to improve the round-trip efficiency.

Molybdenum carbide (Mo_2C) has been widely studied due to its excellent catalytic behavior, similar to that of metals in group VIII, and has attracted extensive attention for methane reforming,[15] the water gas shift reaction,[16] the hydrogen evolution reaction (HER),[17,18] and the CO_2 reduction reaction.[19] Compared with Mo, the high activity of Mo_2C originates from the electronic properties introduced by the carbon, which affects the Mo−C binding energy and the reactivity of adsorbates. Most recently, as the catalyst for Li-O_2 batteries, Mo_2C showed high electrical efficiency and reversibility due to its partially oxidized surface.[20]

In this work, we employed Mo_2C/carbon nanotube (CNT) as the cathode for rechargeable Li-CO_2 batteries. With its three-dimensional (3D) network of uniformly dispersed Mo_2C nanoparticles as catalysis sites and CNTs as the conductive matrix, this cathode material has

reduced the charge plateau below 3.5 V and could be reversibly discharged and charged for 40 cycles. Through a series of ex-situ characterizations, we found that the reversible formation and decomposition of the amorphous discharge product $Li_2C_2O_4$-Mo_2C can reduce charge overpotential and improve the round-trip efficiency of the rechargeable Li-CO_2 battery. The introduction of Mo_2C has set a good example for guiding new catalyst design to improve the energy efficiency of Li-CO_2 batteries.

2. Results and discussion

2.1 Physical Characterization

Molybdenum carbide/carbon nanotube (Mo_2C/CNT) was prepared by the carbothermal reduction of a ball-milled mixture of molybdenum trioxide (MoO_3) and CNT. The ball-milled mixture consists of MoO_3 with particle size in the range of of 200-500 nm and CNTs with a diameter of 10-20 nm (Figure 1a). During the carbothermal reduction, MoO_3 was reduced by the CNT to form Mo_2C. The as-prepared Mo_2C/CNT features a 3D network with uniformly dispersed 50 nm Mo_2C nanoparticles in a CNT framework (Figure 1b), where the Mo_2C particles could serve as catalysis active sites and the CNT matrix could improve the electrical conductivity of the electrode. The crystalline phase compositions of the products were examined by X-ray diffraction (XRD) (Figure 1c). The characteristic peaks of Mo_2C at 34.4, 38.0, 39.4, 52.1, 61.5, 69.6, and 74.6 ° are attributed to the diffractions of the (002), (020), (211), (221), (203), (231), and (223) lattice planes, respectively, which confirms the conversion of MoO_3 into Mo_2C during the carbothermal reduction The carbon peak is substantially diminished when the carbon is consumed. This transition process was also proved by the Raman spectra, which are consistent with the XRD results: the characteristic peaks of Mo_2C/MoO_3 increased while the carbon D-band and G-band peaks were reduced in the Raman spectra (Figure 1d), indicating that CNT was continously consumed during the carbothermal reduction. High-resolution transmission electron microscopy (HRTEM) images

reveal that prepared Mo_2C/CNT holds high crystallinity and well-defined atomic planes (Figure S1, Supporting Information). The planar d (0.149 nm and 0.227 nm) of product is consistent with the (110) and (101) planes of β-Mo_2C, respectively. The CNT and Mo_2C contents of the as-prepared Mo_2C/CNT were further investigated using thermogravimetric analysis (TGA) (Figure S2, Supporting Information), in which CNT was determined to be 5.2% and Mo_2C was determined to be 94.8% Although the molecular ratio of the precursors before carbothermal reduction was strictly adjusted according to the chemical reaction, CNTs still resided in the Mo_2C/CNT, since the efficiency of reduction cannot be 100%. This very low CNT content is not expected to contribute capacity and reactivity with CO_2 at any significant level, although it is still important in suppressing the growth in size of Mo_2C nanoparticles and supplying sufficient electrical conductivity.

2.2 Electrochemical Studies with Mo_2C/CNT

Cyclic voltammetry and galvanostatic cycling were conducted to evaluate battery performance and CO_2 electrode reversibility. The test cells were assembled as described in the Supporting Information (Experimental). Cyclic voltammetry tests were carried out between 2.5 V and 4.2 V (vs. Li/Li^+) at a scan rate of 0.1 mV s^{-1}. As revealed in Figure 2a, Mo_2C/CNT shows a cathodic peak starting from 2.8 V and an anodic peak appearing between 3.4-3.5 V under CO_2. To exclude the background current from the reaction of Mo_2C/CNT in this voltage range, the corresponding test was also conducted under N_2. We found that t no additional Faradic current could be observed, indicating that this pair of peaks observed under CO_2 corresponds to the CO_2 reduction reaction and the CO_2 evolution reaction, respectively. CNT electrode was tested as a comparison, and it shows a cathodic peak and an anodic peak under CO_2 starting from 2.8 V and 4.0 V, respectively, which is a typical response for carbon based electrodes.[14] It is worth noting that the current began to tail off as the potential went above 3.7-3.8 V when Mo_2C/CNT was used as cathode under either N_2 or CO_2, which may be ascribed to the reaction of Mo_2C at such a high voltage. The galvanostatic discharge and

charge of Mo_2C/CNT was tested at the current of 20 μA, in a potential window of 2.0 V- 3.8 V under CO_2. It delivered a reversible capacity of 1150 μAh during discharge and charge, showing that this discharge product can be decomposed below 3.8 V. On the contrary, Mo_2C delivers only 41 μAh under N_2, which indicates that the capacity delivered under CO_2 is related to the reversible CO_2 reduction and evolution process. CNT delivered the capacity of ~2850 μAh during discharge under CO_2, but no capacity was observed under charge process even above 4.0 V, implying that this discharge product cannot be decomposed below 4.0 V. The first cycle galvanostatic discharge-charge curves of CNT electrode and Mo_2C/CNT electrode with a fixed capacity of 100 μAh at the current of 20 μA are presented in Figure 2c, and the round-trip efficiency could be obtained to be 77% when Mo_2C/CNT was used as cathode in Li-CO_2 cells, compared with 60% for the pure CNT electrode. Moreover, the Mo_2C/CNT showed good cycling performance, which lasted for 40 cycles, when it was galvanostatically discharged and charged to 100 μAh at the current of 20 μA (Figure 2d). It was reported that Mo_2C is unstable in Li-O_2 batteries, as it reacts to form a surface layer of MoO_2 on discharge, which appears to result in low charge overpotential, but, in fact, it forms soluble Li_xMoO_3 and leads to electrode degradation.[21] By detecting the change in the separator, we attempted to verify the relation between the discharge/charge process and the stability of Mo_2C in Li-CO_2 batteries. Consistent with the cyclic voltammetry (CV) results, Mo_2C showed stability during discharge and charge to 3.8 V, but it started to dissolve and the separator became dark blue when it was charged above 3.8 V (Figure S3). This finding implies that the soluble species arise from the dissolution of Mo_2C at high voltage, not from the decomposition of the discharge product. By limiting the charge cut-off voltage to 3.65 V, Mo_2C/CNT was fully discharged and charged for three cycles, which showed stable charge potential and good reversibility (Figure S4).

2.3 Ex-situ studies of Mo_2C/CNT electrodes

To understand the different performances of CNT and Mo_2C/CNT in CV and galvanostatic discharge/charge, CNT and Mo_2C/CNT electrodes in different discharge/charge stages were investigated via ex-situ characterizations. It is important to analyse the discharge product and its charging behaviour, which can provide essential insight into the mechanism of rechargeable Li-CO_2 batteries. To obtain the CNT and Mo_2C/CNT materials after discharge, Li-CO_2 cells were discharged to 2.0 V at the current of 20 μA. Typically the cathode was extracted from coin cells in an Ar-filled glove box and rinsed with TEGDME solvent to remove residual $LiCF_3SO_3$ salt. The electrode was then sealed in Kapton tape for protection against air contamination. Based on XRD (Figure S5), SEM (Figure S6), and Raman spectroscopy (Figure S7), the CNT cathode was passivated by crystalline Li_2CO_3 during discharge, which is consistent with previous reports.[6,8,13,14] Unlike CNT electrode, the XRD pattern of discharged Mo_2C/CNT electrode shows that there are no additional new peaks compared with pristine Mo_2C/CNT electrode, indicating that some amorphous product was formed on the surface of Mo_2C/CNT, but not crystalline Li_2CO_3 (Figure S8).

To probe this amorphous discharge product, ex-situ analyses of the surfaces of electrodes at different stages (pristine, discharged, and charged) via SEM, Raman spectroscopy, and X-ray photoelectron spectroscopy (XPS) were carried out. As shown in Figure 3a, the pristine Mo_2C/CNT electrode shows a porous structure, which has the same morphology of Mo_2C/CNT powders. After discharge to 2.0 V, the cathode pores were filled with some film-like material, indicating the formation of an amorphous discharge product on the surface of the Mo_2C/CNT electrode. This film-like product disappeared after the cell was fully charged, indicating the decomposition of this amorphous discharge product. The amorphous morphology and low charge potential may well be linked to a similar phenomenon in the Li-O_2 battery, where it was reported that amorphous peroxide is more ionically conductive than the crystalline phase, and also that there is some superoxide-rich surface which lowers the charge potential.[22,23] To verify the reversible formation and decomposition of the amorphous

product, Raman spectroscopy was carried out to elucidate the electrode compositions and the chemical bonds that are formed and broken (Figure 3b). Two bands of pristine Mo_2C/CNT electrode at 1325 cm^{-1} and 1575 cm^{-1} are respectively assigned to the disorder band (D band) and the graphitic band (G band) of carbon,[24] where the D band and the G band represent the sp^3 C−C single bond and the sp^2 C=C double bond, respectively. After discharge, there is a new peak that appears at 897 cm^{-1}, indicating the formation of a new Mo−O sp^3 hybridization bond.[25] This stretching peak disappears after charge, indicating the breaking of the Mo−O bond. This would suggest that oxygen in CO_2 may combine with molybdenum in Mo_2C to form the amorphous product upon discharge, and this amorphous product releases CO_2 when the Mo−O bond breaks upon charge step. It seems that this strong coupling and the resulting electron delocalisation in the special pair plays a pivotal role in stabilizing such reduced compounds, which can be seen as the Mo−O coupling intermediate.

XPS analysis was further carried out to analyse the oxidation states and composition of the surface of Mo_2C/CNT electrodes in different discharge/charge stages, which was intensively applied to explore the catalysis mechanism, especially for β-Mo_2C.[17–19] The Mo 3d spectra are fitted into $3d_{5/2}$ and $3d_{3/2}$ peaks because of the spin-orbital coupling feature, and the fitting parameters of XPS are shown in Table S1. As shown in Figure 3c, the peak fitting suggests that there are four oxidation states for Mo (Mo^{2+}, Mo^{3+}, Mo^{5+}, Mo^{6+}) on the surface of pristine Mo_2C/CNT electrode. Mo−C bonds in Mo_2C can explain the Mo^{2+} and low oxidation states of Mo^{3+}. Previous studies indicated that the surface of Mo_2C would be contaminated with MoO_2 and MoO_3 when it is exposed to air, which can explain the existence of Mo^{5+} and Mo^{6+}.[17,18] After discharge, the shares of the Mo^{2+}, Mo^{3+}, and Mo^{5+} states were steeply decreased, while that of the Mo^{6+} state rapidly increased, indicating the oxidation of Mo in the low valence state to the high valence state. Consistent with the Raman spectra, the oxidation of Mo in the low valence state to Mo in the high valence state means that Mo acts as an electron donator. The outer electrons of Mo have been transferred to strong electron accepting materials, a role

which should be ascribed to the O atoms in some CO_2 reduction product. Upon charge, the proportions of Mo^{2+}, Mo^{3+}, Mo^{5+}, and Mo^{6+} returned to the initial stage, indicating that the delocalized electrons return to Mo during this reversible charge process. The C 1s spectra (shown in Figure 3d) also show that the C−O peak at 286.6 eV increases after discharge and is reduced after charge, indicating CO_2 capture and release during the discharge/charge process. It is worth noting that no peak related to O−C=O could be observed, indicating that no carbonate radicals are formed during discharge.

2.4 Mechanism of stabilizing the intermediate product by Mo_2C

Compared with the intensive research on the rechargeable Li-O_2 battery, research on the rechargeable Li-CO_2 battery is still an ongoing task. Therefore, some results reported for the Li-O_2 battery may shed light on exploring the mechanism of this new system. It is generally accepted that the reduction in an aprotic Li-O_2 battery proceeds through the general steps shown in Table 1.[26,27] Equations (1-4) show one-electron reduction of O_2 to form O_2^- at the beginning stage, and then a lithium ion combines with O_2^- to form LiO_2, followed by the chemical disproportionation reaction in which LiO_2 disproportionates to Li_2O_2 and O_2, or LiO_2 combines with a lithium ion and an electron to form Li_2O_2. The decomposition of Li_2O_2 will induce high overpotential in the charge process, since it is typically insoluble and electronically insulating. Similarly, in the Li-CO_2 battery, when carbon materials are used as cathode for Li-CO_2 batteries, the discharge product is proved to be Li_2CO_3, and the total reaction can be proposed as:[6,13,14] $4Li^+ + 4e^- + 3CO_2 \rightarrow 2Li_2CO_3 + C$. Although the pathway is still unclear, based on lithium carbonate and carbon as the discharge product, as well as the proved disproportionation of LiO_2 in the Li-O_2 battery, it would be plausibly assumed that some disproportionation reaction takes place in the Li-CO_2 battery, as shown in Table 1.

Table 1. Mechanism of discharge process in the Li-O_2 battery and possible mechanism of discharge process in the Li-CO_2 battery.

Li-O_2 battery		Li-CO_2 battery	
$O_2 + e^- \rightarrow O_2^-$	(1)	$2CO_2 + 2e^- \rightarrow C_2O_4^{2-}$	(5)
$Li^+ + O_2^- \rightarrow LiO_2$	(2)	$C_2O_4^{2-} \rightarrow CO_2^{2-} + CO_2$	(6)
$2LiO_2 \rightarrow Li_2O_2 + O_2$	(3)	$CO_2^{2-} + C_2O_4^{2-} \rightarrow 2CO_3^{2-} + C$	(7)
$LiO_2 + Li^+ + e^- \rightarrow Li_2O_2$	(4)	$2Li^+ + CO_3^{2-} \rightarrow Li_2CO_3$	(8)

Equation (5) shows the one-electron reduction of CO_2 to $C_2O_4^{2-}$ on the surface of carbon materials, for which the open circuit voltage could be calculated to be 3.0 V.[28] It is probable that unstable $C_2O_4^{2-}$ disproportionates through two steps to CO_3^{2-} and C, as shown in Equations (6) and (7). Once crystalline Li_2CO_3 has formed in Equation (8), it is difficult to decompose below 4.0 V.

In the Li-O_2 battery, to reduce charge overpotential, metals in Group VIII such as Ru and Ir were utilized in Li-O_2 battery electrodes.[29-31] It was confirmed that the partial oxidation of the ruthenium facilitates stabilizing the highly unstable peroxide/superoxide ions in the $Li_{2-x}O_2$ phase, and thus reduces the overpotential for Li extraction from the Li_2O_2.[30] Also, the use of Ir-based electrode could absorb and stabilize LiO_2 to become the product of the reaction rather than an intermediate, which dramatically reduces the charge overpotential down to 3.2 V.[31] As it is known to have similar catalytic effects to these metals in Group VIII, Mo_2C probably stabilizes the intermediate product $C_2O_4^{2-}$ on discharge to form an amorphous product, which can be decomposed at low charge potential in the Li-CO_2 battery. Based on experimental results and the similar phenomenon in the Li-O_2 battery, the sequence of proposed possible reaction steps of Mo_2C for rechargeable Li-CO_2 battery are summarized in the following two equations:

$$2CO_2 + 2e^- \rightarrow C_2O_4^{2-} \quad (5)$$

$$C_2O_4^{2-} + 2\,Li^+ + Mo_2C \rightarrow Li_2C_2O_4\text{-}Mo_2C \quad (9)$$

Equation (5) represents the one-electron reduction of CO_2 to $C_2O_4^{2-}$, and the open circuit voltage is calculated to be 3.0 V.[28] In the presence of Mo_2C, some metal-oxygen coupling between Mo in Mo_2C and O in C_2O_4 stabilizes this unstable $C_2O_4^{2-}$ through coordinative electron transfer.[32] This can prevent the formation of insulating Li_2CO_3 and thus easily release CO_2 and Li^+ through uncoupling of the Mo-O chemical bond during charge, which can reduce the charge potential below 3.5 V, as shown in Figure 2b. These reactions can be summarized by the schematic illustration shown in Figure 4. The characteristics that make Mo_2C suitable for this stabilizing function are due to the low valence of molybdenum in Mo_2C, which can promote the transfer of outer electrons to oxygen in the $Li_2C_2O_4$ intermediate product and prevent its disproportionation to Li_2CO_3. So, in the charge process, only amorphous $Li_2C_2O_4$-Mo_2C releases lithium ions and CO_2 below 3.5 V. If crystalline Li_2CO_3 is formed, it cannot be decomposed below 4.0 V. Therefore, Mo_2C is assumed to play an important role in stabilizing the $C_2O_4^{2-}$ as intermediate product, to prevent its further disproportionation reaction.

Moreover, most reported Li-air batteries are actually operated under a pure O_2 atmosphere, while CO_2 and moisture in ambient air can significantly affect the cycling performance when this kind of battery applied in real utilization. As Mo_2C/CNT has been reported as catalyst in Li-O_2 battery,[20] and also has the potential to be used as catalyst with high round-trip efficiency in Li-CO_2 battery, this material may reduce the deleterious impact of CO_2 contamination from air on the cell processes. Thus, although a membrane to avoid moisture is still needed for such an open system, Mo_2C/CNT may hold promise for utilization of Li-air battery under ambient air.

3. **Conclusions**

In summary, Mo_2C/CNT was prepared via a carbothermal reduction process and applied as the catalyst for Li-CO_2 batteries. This composite material shows a high round-trip efficiency of 77%, as well as a good cycling performance. Through a series of characterizations of pure CNT and the as-prepared Mo_2C/CNT, it is clearly shown that CO_2 reduction in the presence of Mo_2C follows a different route that avoids the formation of insulating Li_2CO_3, so to reduce potential plateau on charge and improve round-trip efficiency of rechargeable Li-CO_2 battery. Raman and XPS analysis revealed that the amorphous discharge intermediate product, $Li_2C_2O_4$-Mo_2C, is deposited and decomposed during discharge/charge when Mo_2C/CNT is used as cathode for Li-CO_2 batteries, and it could be well decomposed below 3.5 V. Although further studies using in-situ characterizations are still needed to provide direct evidence for understanding the mechanism behind this reversible reaction, we expect that such an effective catalyst can represent a good example to solve the problems of low electrical efficiency and poor cyclability in Li-CO_2 batteries.

4. **Experimental**

4.1 Synthesis of Mo_2C/CNT materials:

Molybdenum carbide (Mo_2C)/carbon nanotube (CNT) composite material was prepared via carbothermic reduction of a mixture of molybdenum trioxide (MoO_3) and CNTs. In a typical procedure, the starting materials (MoO_3 and CNTs) were accurately weighed according to the stoichiometric amounts for the equation $2MoO_3 + 7C = Mo_2C + 6CO$ and mixed by ball milling for 24 h. The rotation speed and ball-to-powder weight ratio were 300 rpm and 20:1, respectively. To protect the materials from oxidation, the milling operation was carried out under high purity Ar atmosphere. After that, the mixture was heated at 950 °C for 1 h under Ar at the heating rate of 10 °C min^{-1}.

4.2 Preparation of Li-CO_2 batteries:

Mo_2C/CNT (or pure CNT) materials were mixed in N-methyl-2-pyrrolidone (NMP) liquid with a polyvinylidene fluoride binder (PVDF), with a weight ratio of active materials to PVDF of 8:2. The slurry was pasted onto carbon paper disks (diameter of 14 mm) and dried for 12 hours at 120 °C under vacuum to remove the residual solvent. The loading of electrodes was ~4 mg. Electrochemical tests were carried out using coin cells containing the active material working electrode, a lithium metal anode, and electrolyte (1 M $LiCF_3SO_3$ in tetraethylene glycol dimethyl ether (TEGDME) impregnated into a glass fiber separator (Whatman GF/D microfiber filter paper, 2.7 μm pore size). All cell assembly procedures were conducted in an argon-filled glovebox (oxygen and water contents less than 0.1 ppm). Tests were carried out in an CO_2-filled chamber, and before testing, the cells were placed in this CO_2-filled chamber to allow stabilization for 3 hours.

4.3 Physical characterizations

4.3.1 XRD and Microscopy

Powder X-ray diffraction (XRD) was performed on a GBC MMA XRD (λ = 1.54 Å), with the voltage and current kept at − 40 kV and 25 mA, respectively. Scanning electron microscopy (SEM) images were obtained from a JEOL JSM-7500FA field emission SEM, in which the accelerating voltage was set at 5.0 kV and the emission current was 10 mA. Transmission electron microscopy (TEM) investigations were performed using a 200 kV JEOL ARM-200F instrument.

4.3.2 Raman Spectroscopy

Raman spectroscopy was carried out on a Jobin-Yvon Horiba 800 with a 10 mW helium/neon laser at 632.81 nm excitation.

4.3.3 TGA

Thermogravimetric analysis (TGA) was carried out in air using a Q500 (TA Instruments), with data analysis carried out using the Q Series software V. 2.5.0.255. The temperature range studied was between room temperature and 1000 °C, with heating at the rate of 10 °C min^{-1}.

4.3.4 XPS

X-ray photoelectron spectroscopy (XPS) measurements were performed on a VG Scientific ESCALAB 2201XL instrument configured with Al Kα X-ray radiation. All spectra were fitted with Gaussian-Lorentzian functions and a Shirley-type background using CasaXPS software. For the analysis of Mo 3d spectra, constraints were used on the fitting for component pairs: peak area ratio of 2:3 for $3d_{5/2}$: $3d_{3/2}$ and a maximum 0.2 eV difference in the full width half maximum (FWHM). The binding energy values were calibrated using the adventitious C 1s peak at 284.6 eV.

Supporting Information

Supporting Information is available from the Wiley Online Library or from the author.

Acknowledgements

Financial support from an Australian Research Council (ARC) Discovery Project (DP140100401) is gratefully acknowledged. The authors would like to thank the Australian National Fabrication Facility – Materials node and the UOW Electron Microscopy Centre for equipment use, with particular thanks to Dr. Prof Wu would appreciate financial support from National Materials Genome Project (2016YFB0700600), Nationl Distinguished Young Scientists Program (51425301) and NSFC (21374021 and U1601214). David Mitchell. Many thanks also go to Dr. Tania Silver for critical reading of the manuscript.

Received: ((will be filled in by the editorial staff))
Revised: ((will be filled in by the editorial staff))
Published online: ((will be filled in by the editorial staff))

References

[1] T. M. McDonald, J. A. Mason, X. Kong, E. D. Bloch, D. Gygi, A. Dani, V. Crocellà, F. Giordanino, S. O. Odoh, W. S. Drisdell, B. Vlaisavljevich, A. L. Dzubak, R. Poloni, S. K. Schnell, N. Planas, K. Lee, T. Pascal, L. F. Wan, D. Prendergast, J. B. Neaton, B. Smit, J. B. Kortright, L. Gagliardi, S. Bordiga, J. A. Reimer, J. R. Long, *Nature* **2015**, *519*, 303.

[2] J. Liu, P. K. Thallapally, B. P. McGrail, D. R. Brown, J. Liu, *Chem. Soc. Rev.* **2012**, *41*, 2308.

[3] W. Choi, K. Min, C. Kim, Y. S. Ko, J. W. Jeon, H. Seo, Y.-K. Park, M. Choi, *Nat. Commun.* **2016**, *7*, 12640.

[4] S. Gao, X. Jiao, Z. Sun, W. Zhang, Y. Sun, C. Wang, Q. Hu, X. Zu, F. Yang, S. Yang, L. Liang, J. Wu, Y. Xie, *Angew. Chemie - Int. Ed.* **2016**, *55*, 698.

[5] K. Takechi, T. Shiga, T. Asaoka, *Chem. Commun.* **2011**, *47*, 3463.

[6] S. Xu, S. K. Das, L. Archer, *RSC Adv.* **2013**, *3*, 6656.

[7] H.-K. Lim, H.-D. Lim, K.-Y. Park, D.-H. Seo, H. Gwon, J. Hong, W. A. Goddard, H. Kim, K. Kang, *J. Am. Chem. Soc.* **2013**, *135*, 9733.

[8] Y. Liu, R. Wang, Y. Lyu, H. Li, L. Chen, *Energy Environ. Sci.* **2014**, *7*, 677.

[9] X. Li, S. Yang, N. Feng, P. He, H. Zhou, *Chinese Journal of Catalysis*. **2016**, *37*, 1016.

[10] X. Zhang, X.-G. Wang, Z. Xie, Z. Zhou, *Green Energy & Environment* **2016**, *1*, 4.

[11] Z. Xie, X. Zhang, Z. Zhang, Z. Zhou, *Adv. Mater*. **2017**, 1605891.

[12] S. Yang, P. He, H. Zhou, *Energy Environ. Sci*. **2016**, *9*, 1650.

[13] X. Zhang, Q. Zhang, Z. Zhang, Y. Chen, Z. Xie, J. Wei, Z. Zhou, *Chem. Commun.* **2015**, *51*, 14636.

[14] Z. Zhang, Q. Zhang, Y. Chen, J. Bao, X. Zhou, Z. Xie, J. Wei, Z. Zhou, *Angew. Chemie - Int. Ed.* **2015**, *54*, 6550.

[15] K. Oshikawa, M. Nagai, S. Omi, *J. Phys. Chem. B* **2001**, *105*, 9124.

[16] N. M. Schweitzer, J. A. Schaidle, O. K. Ezekoye, X. Pan, S. Linic, L. T. Thompson, *J. Am. Chem. Soc.* **2011**, *133*, 2378.

[17] C. Wan, Y. N. Regmi, B. M. Leonard, *Angew. Chemie - Int. Ed.* **2014**, *53*, 6407.

[18] H. Vrubel, X. Hu, *Angew. Chemie - Int. Ed.* **2012**, *51*, 12703.

[19] M. D. Porosoff, X. Yang, J. A. Boscoboinik, J. G. Chen, *Angew. Chemie - Int. Ed.* **2014**, *53*, 6705.

[20] W. Kwak, K. C. Lau, C. Shin, K. Amine, L. A. Curtiss, Y. Sun, *ACS Nano* **2015**, *9*, 4129.

[21] D. Kundu, R. Black, B. Adams, K. Harrison, K. Zavadil, L. F. Nazar, *J. Phys. Chem. Lett.* **2015**, *6*, 2252.

[22] Y. Zhang, Q. Cui, X. Zhang, W. C. McKee, Y. Xu, S. Ling, H. Li, G. Zhong, Y. Yang, Z. Peng, *Angew. Chemie - Int. Ed.* **2016**, *55*, 10717.

[23] J. Yang, D. Zhai, H.-H. Wang, K. C. Lau, J. A. Schlueter, P. Du, D. J. Myers, Y.-K. Sun, L. A. Curtiss, K. Amine, *Phys. Chem. Chem. Phys.* **2013**, *15*, 3764.

[24] J.-S. Li, Y. Wang, C.-H. Liu, S.-L. Li, Y.-G. Wang, L.-Z. Dong, Z.-H. Dai, Y.-F. Li, Y.-Q. Lan, *Nat. Commun.* **2016**, *7*, 11204.

[25] R. H. Busey, O. L. Keller, *J. Chem. Phys.* **1964**, *41*, 215.

[26] L. Johnson, C. Li, Z. Liu, Y. Chen, S. Freunberger, P. C. Ashok, B. B. Praveen, K. Dholakia, J.-M. Tarascon, P. G. Bruce, *Nat. Chem.* **2014**, *6*, 1091.

[27] J. S. Hummelshøj, A. C. Luntz, J. K. Nørskov, *J. Chem. Phys.* **2013**, *138*, 0.

[28] K. Németh, G. Srajer, *RSC Adv.* **2014**, *4*, 1879.

[29] J. Jiang, P. He, S. Tong, M. Zheng, Z. Lin, X. Zhang, Y. Shi, H. Zhou, *NPG Asia Materials* **2016**, *8*, e239.

[30] Y. Wang, Z. Liang, Q. Zou, G. Cong, Y. C. Lu, *J. Phys. Chem. C* **2016**, *120*, 6459.
[31] J. Lu, Y. Jung Lee, X. Luo, K. Chun Lau, M. Asadi, H.-H. Wang, S. Brombosz, J. Wen, D. Zhai, Z. Chen, D. J. Miller, Y. Sub Jeong, J.-B. Park, Z. Zak Fang, B. Kumar, A. Salehi-Khojin, Y.-K. Sun, L. A. Curtiss, K. Amine, *Nature* **2016**, *529*, 1.
[32] R. Angamuthu, P. Byers, M. Lutz, A. L. Spek, E. Bouwman, *Science* **2010**, *327*, 313.

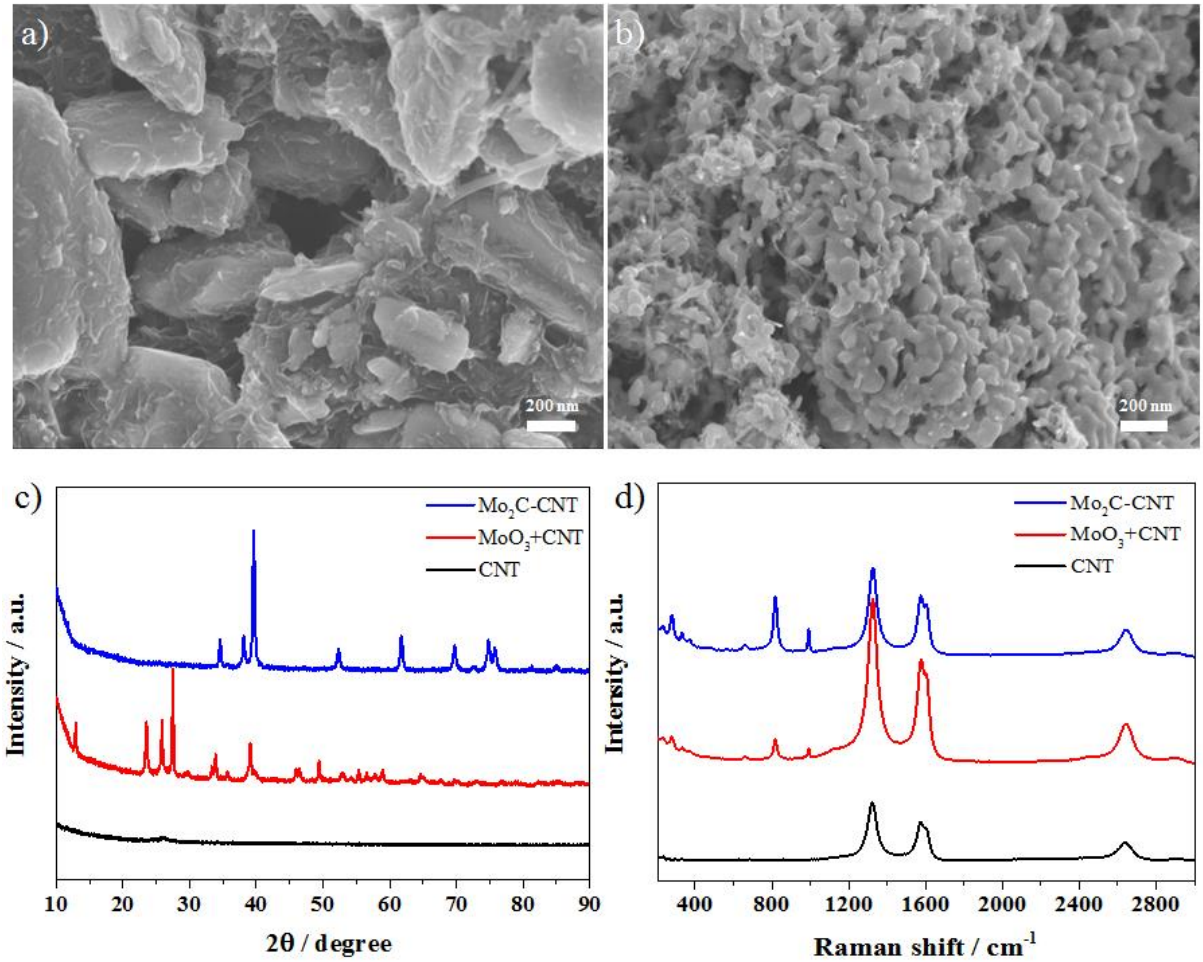

Figure 1 (a) Scanning electron microscope (SEM) image of precursor mixture of MoO_3 and CNT after ball milling (scale bar: 200 nm); (b) SEM image of as-prepared Mo_2C/CNT after carbothermal reduction (scale bar: 200 nm); (c) XRD patterns of the precursor mixture of MoO_3 and CNT, pure CNT, and as-prepared Mo_2C/CNT; (d) Raman spectra of the precursor mixture of MoO_3 and CNT, pure CNT, and as-prepared Mo_2C/CNT.

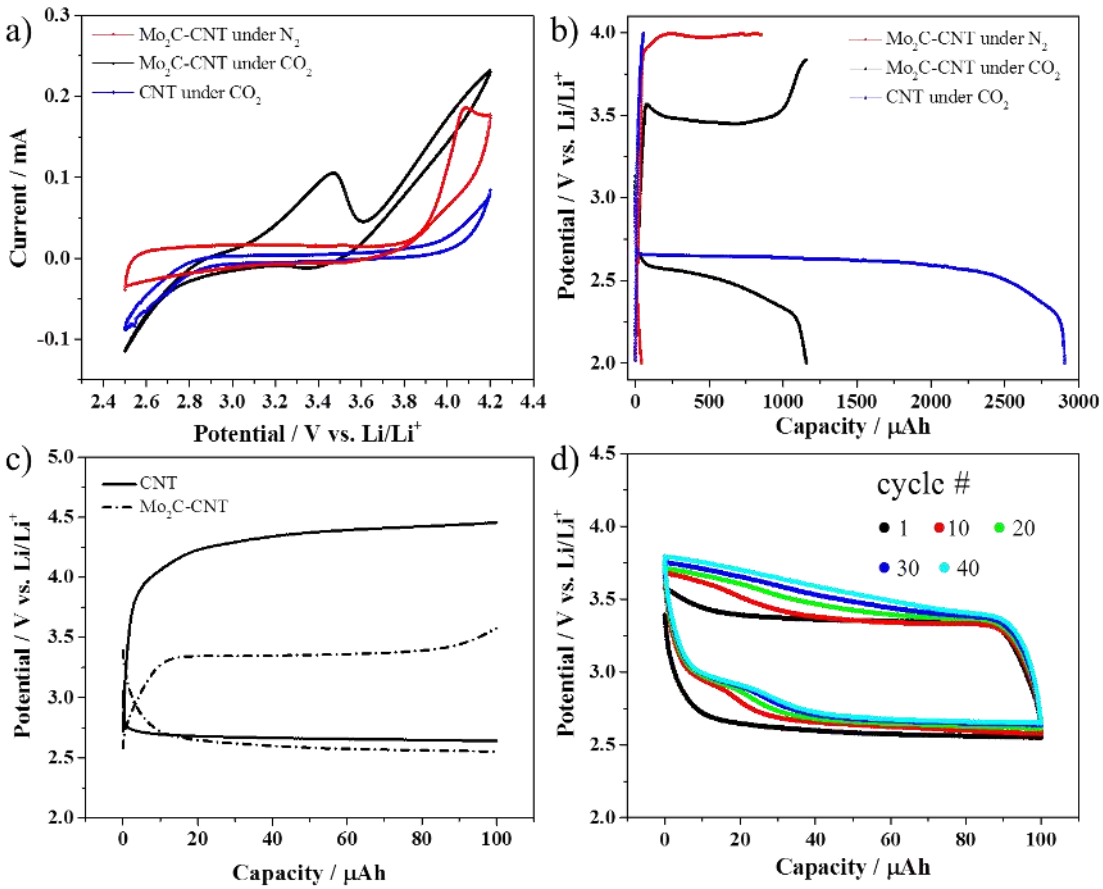

Figure 2. (a) Cyclic voltammograms (CV) of Mo_2C/CNT electrodes under N_2 and CO_2, and CNT electrode under CO_2. Counter and reference electrodes: Li metal. Scan rate: 0.1 mV s^{-1}. Voltage window: 2.5 V - 4.2 V vs. Li/Li^+. (b) Galvanostatic discharge-charge profiles of Mo_2C/CNT electrodes under N_2 and CO_2, and CNT electrode under CO_2 with the current at 20 µA. (c) Galvanostatic discharge-charge profiles of CNT and Mo_2C/CNT electrodes under CO_2 at the current of 20 µA, up to the capacity of 100 µAh. (d) Cycling performance of Mo_2C/CNT electrode for selected cycles under CO_2 at the current of 20 µA, up to the capacity of 100 µAh.

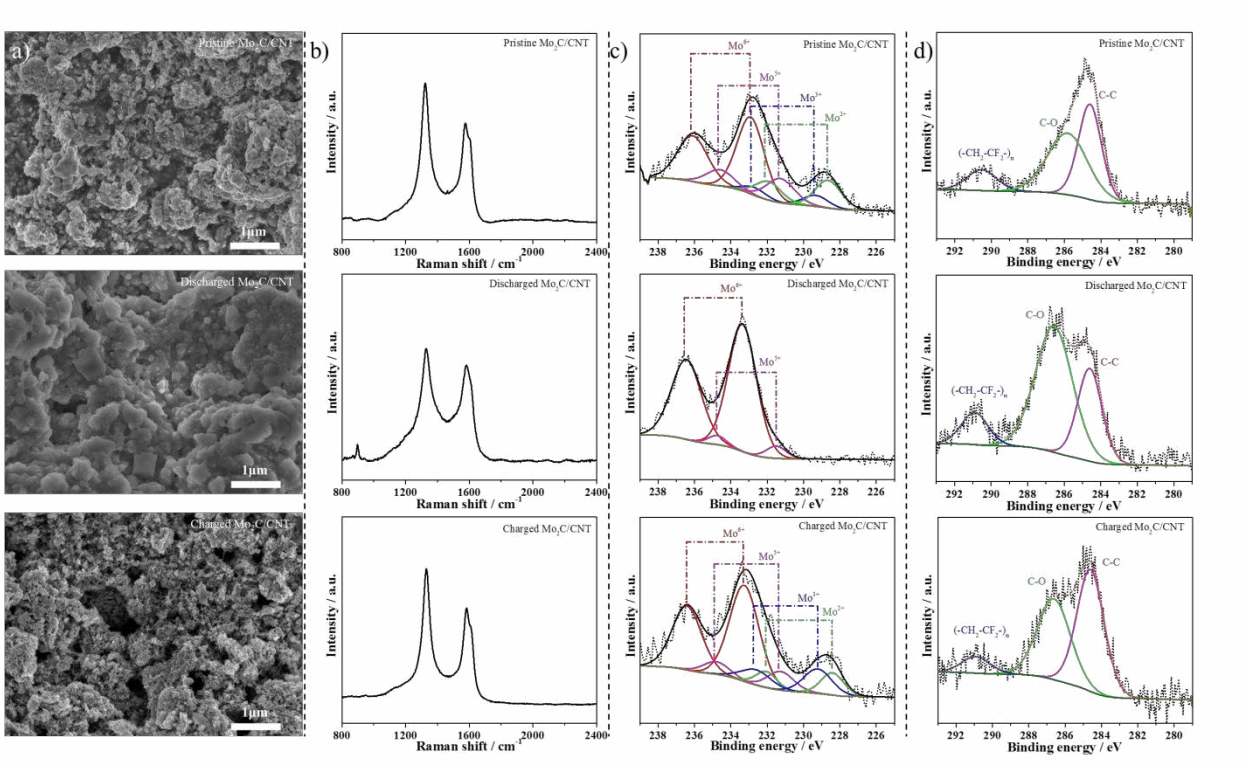

Figure 3 (a) SEM images of Mo_2C/CNT electrode at different stages: pristine (top), discharged (middle), charged (bottom); (b) Raman spectra of Mo_2C/CNT electrode at different stages: pristine (top), discharged (middle), charged (bottom); (c) X-ray photoelectron spectra (XPS) of Mo 3d for Mo_2C/CNT electrode at different stages: pristine (top), discharged (middle), charged (bottom); d) X-ray photoelectron spectra (XPS) of C 1s for Mo_2C/CNT electrode at different stages: pristine (top), discharged (middle), charged (bottom).

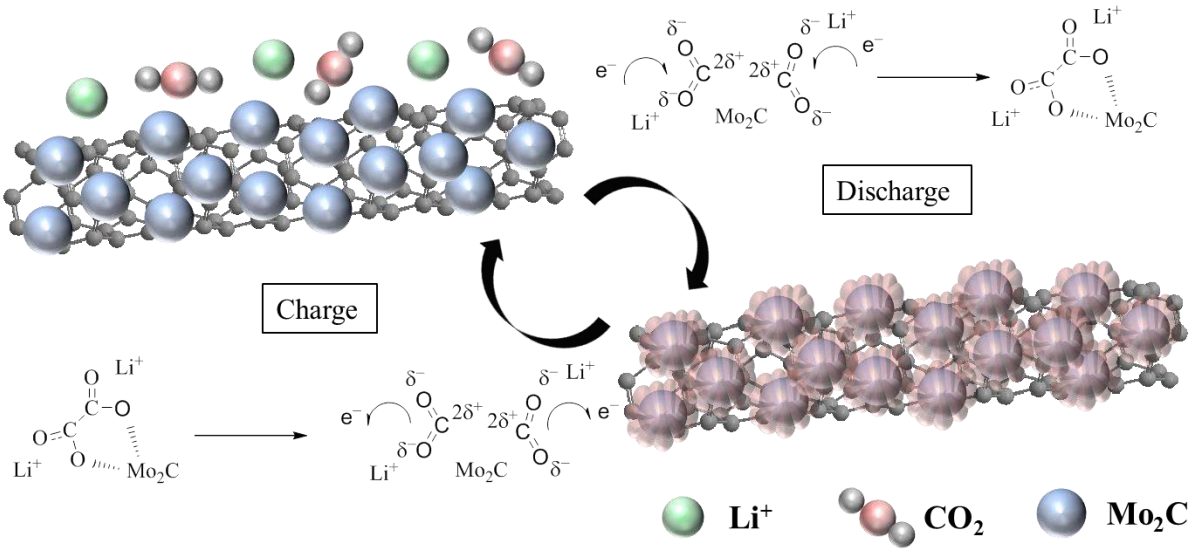

Figure 4. Schematic illustration of reactions during discharge and charge of Mo_2C/CNT in the Li-CO_2 battery. CO_2 is reduced at the Mo_2C/CNT electrode surface on discharge, forming $Li_2C_2O_4$, and then this intermediate product is stabilized by Mo_2C, forming an amorphous discharge product that can be easily decomposed on charge.

ToC figure

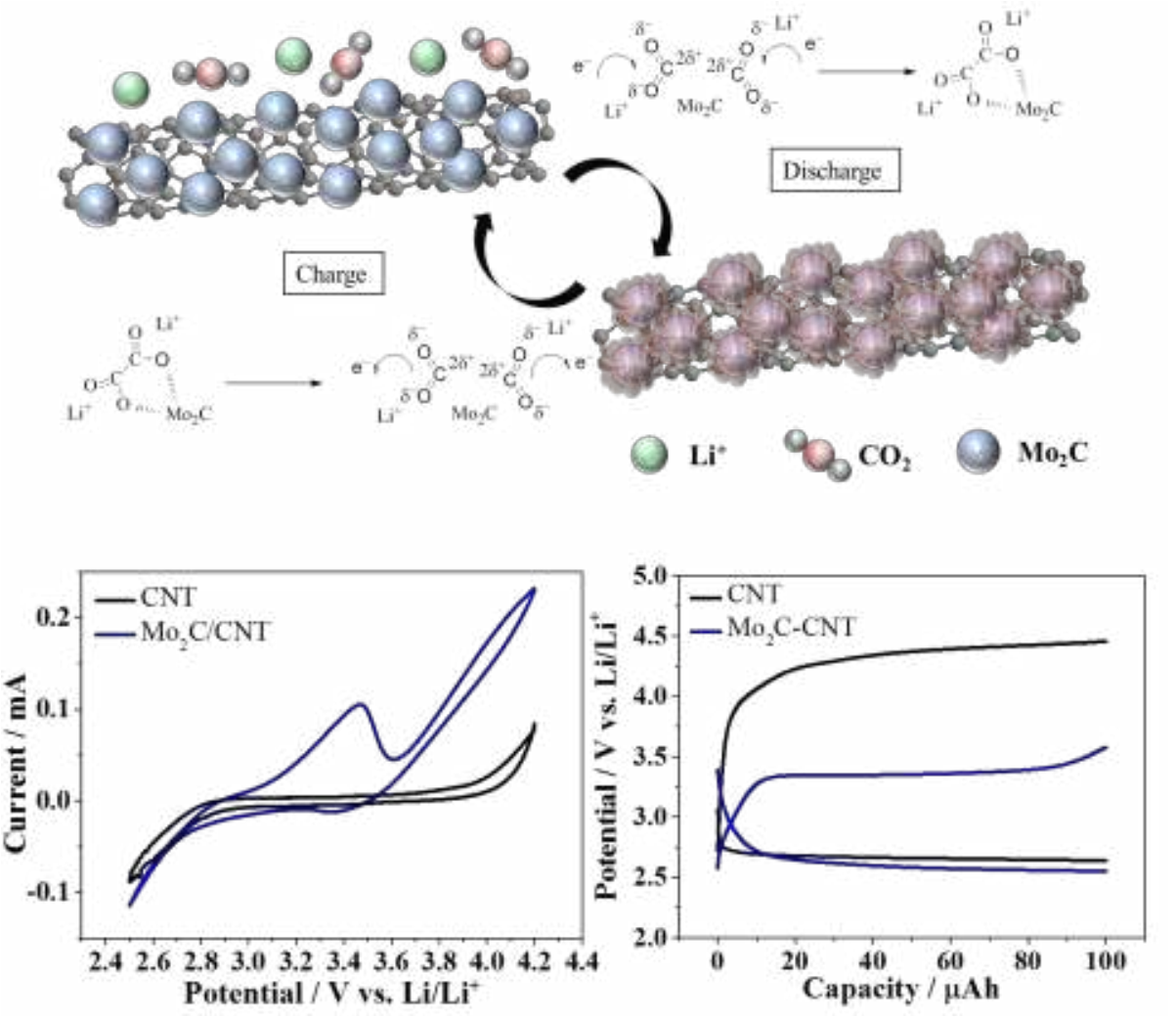
Discharge
Charge
Li+
CO2
Mo2C
CNT
Mo2C/CNT
Current / mA
Potential / V vs. Li/Li+
CNT
Mo2C-CNT
Potential / V vs. Li/Li+
Capacity / μAh

Supporting Information

Mo_2C/CNT as an Efficient Catalyst for Rechargeable Li-CO_2 Batteries

Yuyang Hou[1], Jiazhao Wang[2,], Lili Liu[2], Yuqing Liu[1], Shulei Chou[2], Dongqi Shi[2], Huakun Liu[2], Yuping Wu[3], Weimin Zhang[4], Jun Chen[1,*]*

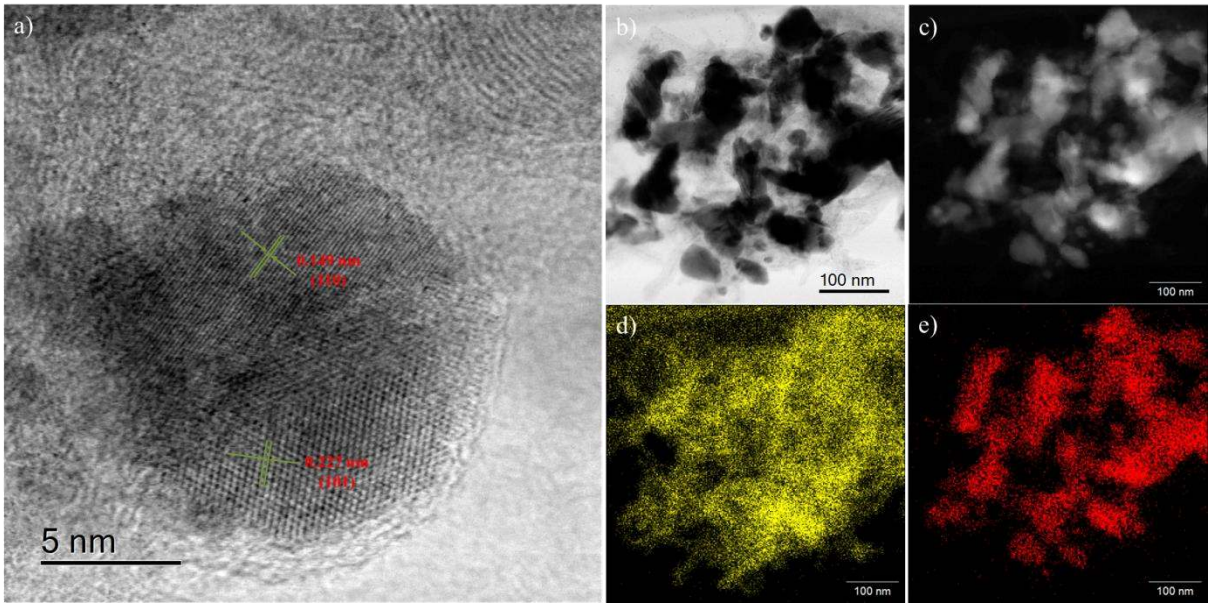

Figure S1. a) The HRTEM image of nanoparticle of as-prepared Mo_2C/CNT composite material; b-e) EDS with HRTEM in a highly resolved small area of Mo_2C/CNT (yellow: C, red: Mo).

The high-resolution TEM (HRTEM) image indicates that the particles possess a typical crystalline texture, with space between lattice planes of 0.149 nm and 0.227, which corresponds to the d value of the (110) and (101) planes of Mo_2C, which can well confirm the results of our XRD and SEM.

The EDS with HRTEM in a highly resolved small area of Mo_2C/CNT shows the morphology and shape of as prepared Mo_2C/CNT, and this mapping analysis also shows uniformity of Mo and C elements.

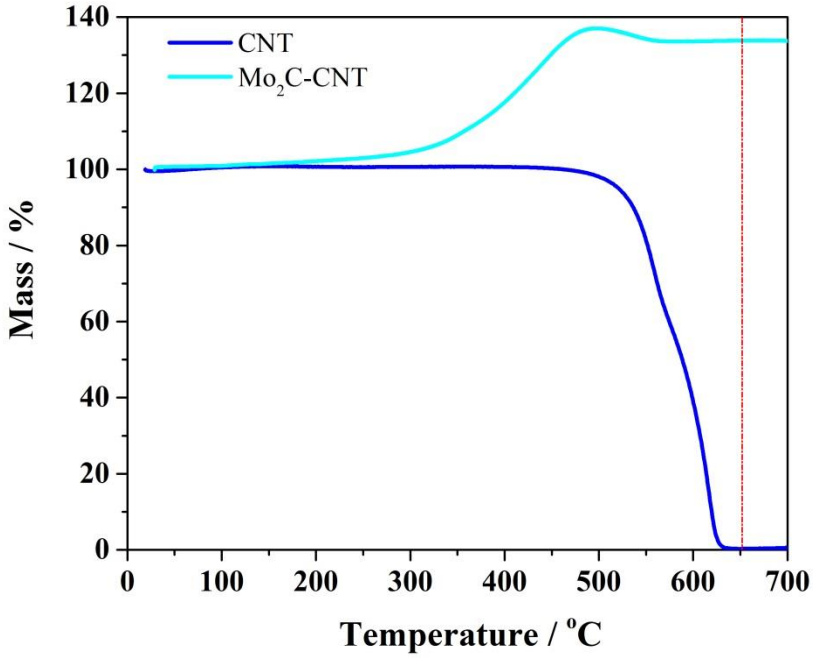

Figure S2. TGA curves of CNT and Mo_2C/CNT, indicating that Mo_2C was completely transformed into MoO_3 while the CNT was transformed into CO_2.

In the TGA curve of Mo_2C/CNT, the initial weight gain from 300 °C to 500 °C is attributed to the gradual oxidation of Mo_2C to MoO_3, followed by a slight weight loss caused by the combustion of CNTs. When Mo_2C/CNT is heated to 700 °C, it is completely transformed into MoO_3. According to these results, the Mo_2C content is estimated to be 94.8 wt.% in Mo_2C/CNT, based on the following equation: m (Mo_2C) = 133.8 wt.% * M(Mo_2C)/2M(MoO_3) = 94.8 wt.%, and the CNT content is calculated to be 5.2 wt. %

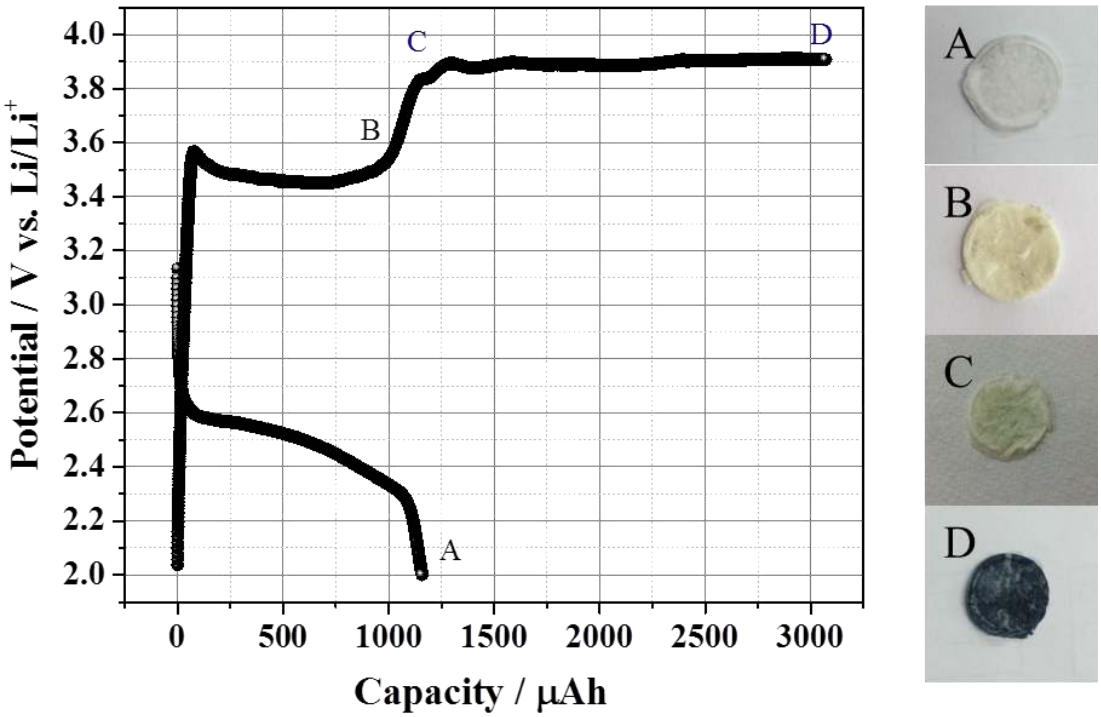

Figure S3. Galvanostatic discharge and charge profile (left) of the Mo_2C/CNT cathode in a Li-CO_2 cell, and corresponding images of separators taken out of the battery at the indicated stages (right).

Typically, a Li-CO_2 battery with Mo_2C/CNT as cathode was discharged to 2.0 V, as shown in step A, at which point the separator was clean, indicating that the battery is stable during discharge; it was then charged to 3.65 V at step B, at which the separator was still clean, indicating that the decomposition of discharge product is stable; the battery was then charged to the capacity delivered upon discharge at step C, at which the separator was slightly blue, indicating full decomposition of the discharge product, although the electrode started to decompose at this voltage; the battery was finally charged to 3100 μAh at step D, at which the separator was dark blue, indicating that the Mo_2C had become unstable and was starting to dissolve in electrolyte above 3.8 V, as also proved by the stable voltage plateau.

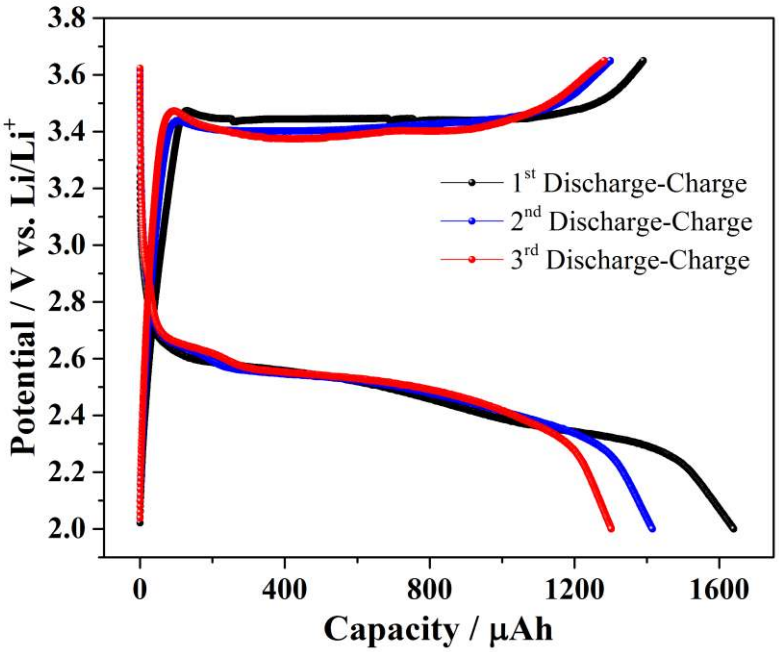

Figure S4. Galvanostatic cycling for the first 3 cycles of the Mo_2C/CNT cathode in a Li-CO_2 cell at the current of 20 µA in a 2.0 V – 3.65 V (vs. Li/Li^+) voltage window. 20 µA of current was applied for both discharge and charge. Although there is still degradation during cycling, this might have come from insufficient decomposition of the discharge product.

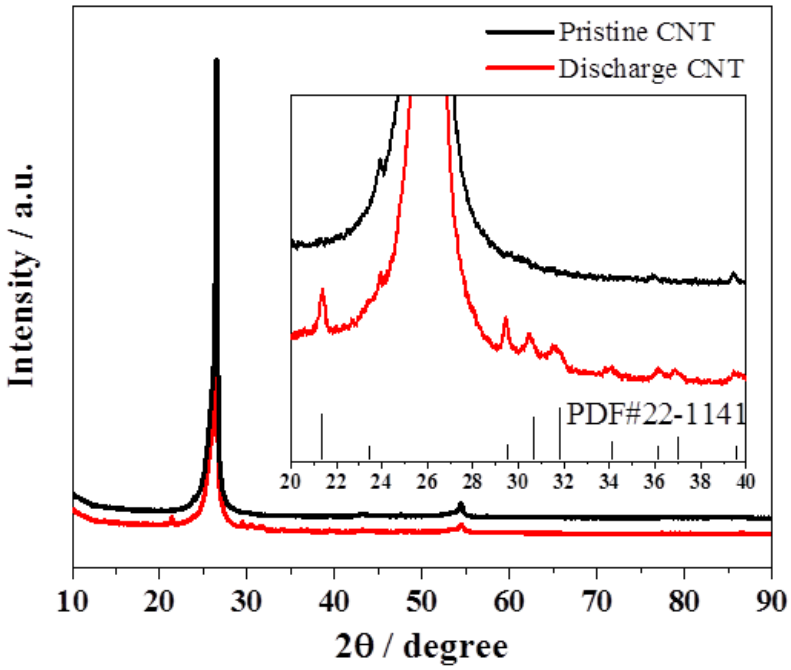

Figure S5. XRD pattern of CNT electrodes at different stages (pristine CNT: black line; and discharged CNT: red line), with the inset showing an enlargement of the indicated range.

The carbon paper exhibited the typical graphite structure, with a sharp (002) XRD graphite peak at $2\theta \approx 26.55°$ and a small (004) XRD graphite peak at $2\theta \approx 54.75°$. After discharge, some characteristic peaks appeared, which correspond to the formation of Li_2CO_3, according to XRD card PDF#22-1141.

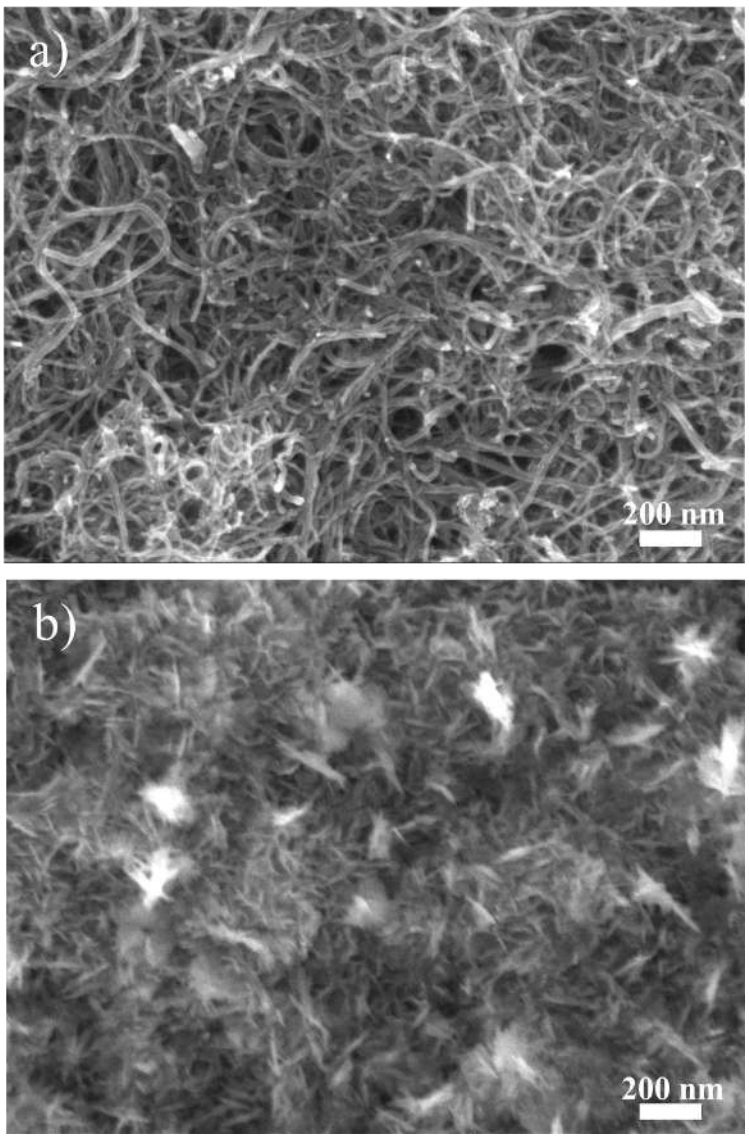

Figure S6. SEM images of CNT electrode at different stages: (a) pristine CNT; (b) discharged CNT.

The pristine CNT features a homogeneous crosslinked structure, with the diameters of the nanotubes in the range of 10-20 nm. After discharge to 2.0 V at the current of 20 μA, the crosslinked structure was filled with some plate-like product.

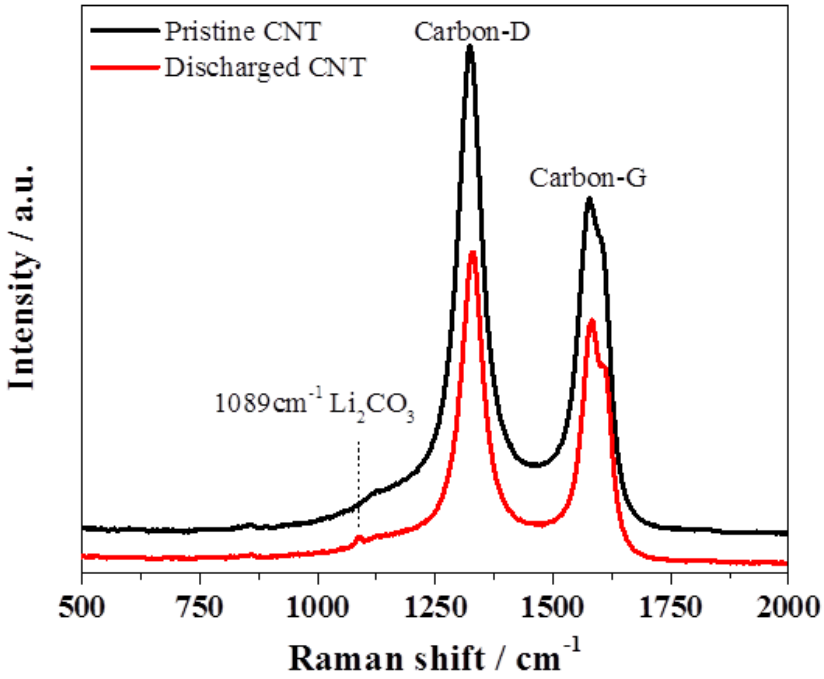

Figure S7. Raman spectra of CNT electrodes at different stages (pristine CNT: black line; discharged CNT: red line).

The D band and G band are clearly shown in the Raman spectra, which should be ascribed to the CNT. Compared with the pristine CNT, there is a new peak at 1089 cm^{-1}, corresponding to the formation of Li_2CO_3.

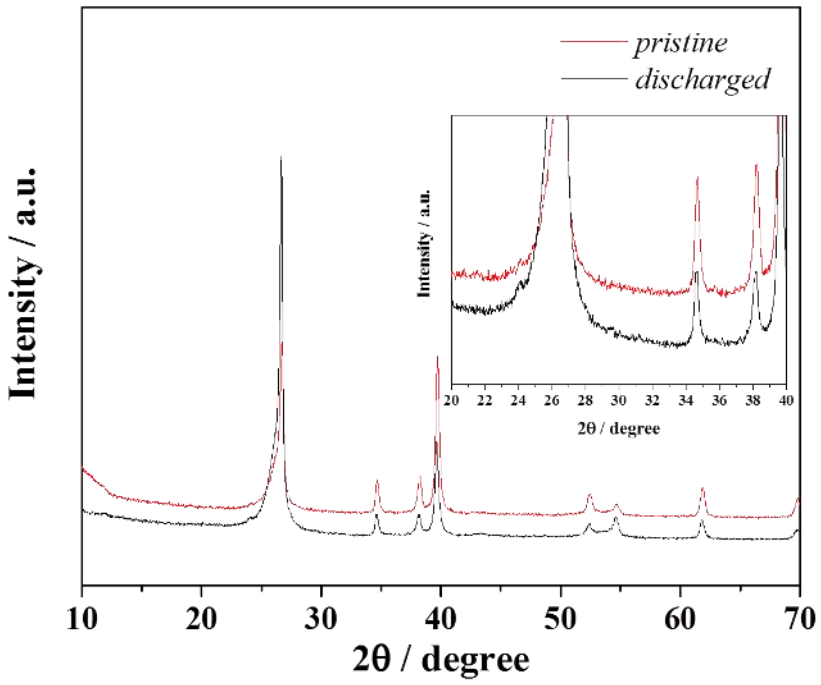

Figure S8. XRD patterns of Mo_2C/CNT electrodes at different stages (pristine Mo_2C/CNT: black line; discharged Mo_2C/CNT: red line), with the inset showing an enlargement of the indicated range.

Unlike discharged CNT in a Li-CO_2 cell, no additional new peaks appeared when Mo_2C/CNT was used as cathode in a Li-CO_2 cell, indicating that no crystalline Li_2CO_3 was formed during discharge.

Table S1 Fitting parameters (peak position, full width at half maximum (FWHM), and species percentage) for both Mo $3d_{3/2}$ and Mo $3d_{5/2}$ spectra collected from Mo_2C/CNT electrode in different stages (pristine, discharged, charged).

Electrode	Species	Peak position for Mo $3d_{5/2}$ (former); Mo $3d_{3/2}$ (latter) / eV	FWHM for Mo $3d_{5/2}$ (former); Mo $3d_{3/2}$ (latter) / eV	Species percentage / %
Pristine Mo_2C/CNT	Mo^{2+}	228.64; 231.92	1.69; 1.67	19.3
	Mo^{3+}	229.33; 232.69	1.61; 1.51	7.4
	Mo^{5+}	231.26; 234.60	1.81; 1.79	18.0
	Mo^{6+}	232.91; 236.09	1.76; 1.96	55.3
Discharged Mo_2C/CNT	Mo^{2+}	-	-	-
	Mo^{3+}	-	-	-
	Mo^{5+}	231.50; 234.74	1.28; 1.15	6.4
	Mo^{6+}	233.35; 236.44	1.82; 1.93	93.6
charged Mo_2C/CNT	Mo^{2+}	228.40; 232.05	1.48; 1.37	11.3
	Mo^{3+}	229.21; 232.61	1.80; 1.93	15.2
	Mo^{5+}	231.26; 234.80	1.71; 1.70	11.9
	Mo^{6+}	233.25; 236.41	1.90; 1.90	62.6